AGU PUBLICATIONS

Geophysical Research Letters

RESEARCH LETTER
10.1002/2016GL068064

Key Points:
- Precipitation response from five climate drivers shown for nine climate models
- Fast responses scale with atmospheric absorption, slow with surface temperature
- Over some land regions, fast precipitation responses dominate the slow response

Supporting Information:
- Figures S1 and S2 and captions for Tables S1 and S2
- Table S1

Correspondence to:
B. H. Samset,
b.h.samset@cicero.oslo.no

Citation:
Samset, B. H., et al. (2016), Fast and slow precipitation responses to individual climate forcers: A PDRMIP multimodel study, *Geophys. Res. Lett., 43*, 2782–2791, doi:10.1002/2016GL068064.

Received 2 FEB 2016
Accepted 19 FEB 2016
Accepted article online 25 FEB 2016
Published online 16 MAR 2016

Fast and slow precipitation responses to individual climate forcers: A PDRMIP multimodel study

B. H. Samset[1], G. Myhre[1], P. M. Forster[2], Ø. Hodnebrog[1], T. Andrews[3], G. Faluvegi[4], D. Fläschner[5], M. Kasoar[6], V. Kharin[7], A. Kirkevåg[8], J.-F. Lamarque[9], D. Olivié[8], T. Richardson[2], D. Shindell[10], K. P. Shine[11], T. Takemura[12], and A. Voulgarakis[6]

[1]Center for International Climate and Environmental Research, Oslo, Norway, [2]School of Earth and Environment, University of Leeds, Leeds, UK, [3]Met Office Hadley Centre, Exeter, UK, [4]NASA Goddard Institute for Space Studies, New York, New York, USA, [5]Max-Planck-Institut für Meteorologie, Hamburg, Germany, [6]Faculty of Natural Sciences, Department of Physics, Imperial College London, London, UK, [7]Canadian Centre for Climate Modelling and Analysis, Gatineau, Quebec, Canada, [8]Norwegian Meteorological Institute, Oslo, Norway, [9]NCAR/UCAR, Boulder, Colorado, USA, [10]Nicholas School of the Environment, Duke University, Durham, North Carolina, USA, [11]Department of Meteorology, University of Reading, Reading, UK, [12]Research Institute for Applied Mechanics, Kyushu University, Fukuoka, Japan

Abstract Precipitation is expected to respond differently to various drivers of anthropogenic climate change. We present the first results from the Precipitation Driver and Response Model Intercomparison Project (PDRMIP), where nine global climate models have perturbed CO_2, CH_4, black carbon, sulfate, and solar insolation. We divide the resulting changes to global mean and regional precipitation into fast responses that scale with changes in atmospheric absorption and slow responses scaling with surface temperature change. While the overall features are broadly similar between models, we find significant regional intermodel variability, especially over land. Black carbon stands out as a component that may cause significant model diversity in predicted precipitation change. Processes linked to atmospheric absorption are less consistently modeled than those linked to top-of-atmosphere radiative forcing. We identify a number of land regions where the model ensemble consistently predicts that fast precipitation responses to climate perturbations dominate over the slow, temperature-driven responses.

1. Introduction

Global precipitation levels and patterns are changing in response to global warming [*Hartmann et al.*, 2013]. Climate change is presently caused by the interaction of drivers such as changing concentrations of greenhouse gases, natural and anthropogenic aerosol emissions, and changes to solar insolation [*Myhre et al.*, 2013a]. While the connection between a changing temperature and the hydrological cycle may be understood through energy balance analyses [*Allen and Ingram*, 2002; *O'Gorman et al.*, 2012], future precipitation changes are poorly constrained in state of the art climate models [*Collins et al.*, 2013; *Knutti and Sedláček*, 2012]. Present models also tend to underestimate the solar absorption response to changes in water vapor following a climate perturbation, overestimating the resulting change in global mean precipitation [*DeAngelis et al.*, 2015]. Even when identically perturbed by an ensemble of climate forcers, differences in present models' individual atmospheric responses to these forcers give rise to significant uncertainties. Improving such precipitation forecasts, both globally and regionally, and on short and long time scales, is an important topic in present climate research, since precipitation is one of the climate factors that most closely affects human society.

The global apparent hydrological sensitivity, defined as the total change in precipitation per degree of global warming, differs between climate drivers such as CO_2 and solar insolation [*Allen and Ingram*, 2002]. Further, the precipitation response to a climate forcer is usually thought to happen on two time scales: a rapid adjustment of the atmosphere to the change in energy balance as a direct result of the climate driver and one slower response, scaling with the change in surface temperature [see, e.g., *Boucher et al.*, 2013; *Cao et al.*, 2012; *Kamae and Watanabe*, 2012; *Myhre et al.*, 2013a; *Sherwood et al.*, 2015]. The realization that these processes may be very differently represented in models led to the suggestion [*Bala et al.*, 2010] that fast and slow responses be compared separately in multimodel intercomparisons to uncover robust responses in the hydrological cycle. Other publications have noted that the slow precipitation change per degree of warming is well constrained, indicating that the main differences in apparent response lie in the rapid adjustments [*Andrews and Forster*, 2010; *Fläschner et al.*, 2016].

Recently, several single-model studies have investigated the response to climate drivers in isolation. *Andrews et al*. [2010] forced the HadGEM1 model with greenhouse gas, aerosol, albedo, and solar insolation perturbations. They found strong correlations between the top-of-atmosphere forcing of a perturbation and the slow, temperature-driven precipitation change and between the modeled atmospheric absorption and the fast precipitation change. *Kvalevåg et al*. [2013] repeated the studies using the National Center for Atmospheric Research (NCAR) CESM1 model and the CAM4 atmospheric component. They found very similar overall results and correlations to *Andrews et al*. [2010] but a number of significant differences in response to otherwise identical climate perturbations.

No coordinated effort has, however, yet been made to compare the precipitation response to identical single-driver perturbations across a broad range of models. To perform such a comparison was the formative idea behind the Precipitation Driver and Response Model Intercomparison Project (PDRMIP). In the following sections, we present the first results of the PDRMIP effort, based on results reported by nine global climate models. The experiment design broadly follows that used in *Andrews et al*. [2010] and *Kvalevåg et al*. [2013], but with some differences implemented in order to allow as many models as possible to apply identical perturbations to their climate simulations. The details of the PDRMIP setup, aerosol distributions, and simulations will be covered in a separate publication. Here we present the first analysis of the PDRMIP precipitation responses to five climate drivers and extend the analysis to separate the responses over ocean and various land regions. Upcoming publications will further explore the hydrological sensitivities, energy balances, and circulation changes that underlie the present results.

2. Methods

In PDRMIP, global coupled climate models have performed simulations with comparable configurations, forcing baseline, and equilibrated climates with individual drivers. In the following, we define the perturbations, present the participating models, and show how the temperature, precipitation, and radiative forcing responses were calculated. The models used for the present analysis are CanESM2, NorESM1, HadGEM2, HadGEM3-GA4, GISS-E2, NCAR CESM1 CAM4, NCAR CESM1 CAM5, MPI-ESM, and MIROC-SPRINTARS (see Table S1 in the supporting information for details and model references).

For the present analysis, five perturbations were simulated: a doubling of CO_2 concentration (hereafter denoted *CO2x2*), tripling of CH_4 concentration (*CH4x3*), 2% increase in solar insolation (*Sol + 2%*), 10 times black carbon (BC) concentration or emissions (*BCx10*), and 5 times SO_4 concentrations or emissions (*SO4x5*). All perturbations were abrupt, relative to present-day or preindustrial values. Greenhouse gas and solar insolation perturbations were applied relative to the models' own baseline values. For the aerosol perturbations, multimodel mean monthly present-day concentrations were extracted from the submissions to AeroCom Phase II [see, e.g., *Myhre et al*., 2013b; *Samset et al*., 2013]. To form perturbations, they were multiplied by the stated factor, and both baseline and perturbed fields were regridded to the native resolution of the PDRMIP models. Some models were, however, unable to perform simulations with prescribed concentrations. These models instead ran a baseline with present-day emissions and then multiplied these emissions by the prescribed factors.

For the baseline and each perturbation, each model ran two sets of simulations: one keeping sea surface temperatures fixed (hereafter denoted *f*SST) and one with a slab ocean or fully coupled ocean (*coupled*). The *f*SST simulations were run for 15 years and the coupled simulations for 100 years. Only one ensemble member was used for each model. Note that for the present analysis, focusing on subcentennial responses, the use of a long simulation with constant forcings is equivalent to a perturbed initial-condition ensemble.

Table S1 summarizes the nine models that were used for the present analysis, including their ocean setup and native resolutions, and whether they used emissions or prescribed aerosol concentrations. All models simulated all perturbations, except MPI-ESM which did not have the capability for performing the aerosol perturbations. One model (CESM-CAM4) used a slab ocean setup for the coupled simulations, and the others used a full ocean representation.

Radiative forcing (RF) due to a climate perturbation was diagnosed using the difference in global mean flux for years 6–15 from the *f*SST simulations. The analysis was performed at top-of-atmosphere (TOA, RF_{TOA}) and at the surface (RF_{surf}). The change in atmospheric absorption due to the climate perturbation was then defined as $\text{Atm.abs.} = RF_{TOA} - RF_{surf}$. The run length was determined based on earlier observations that the

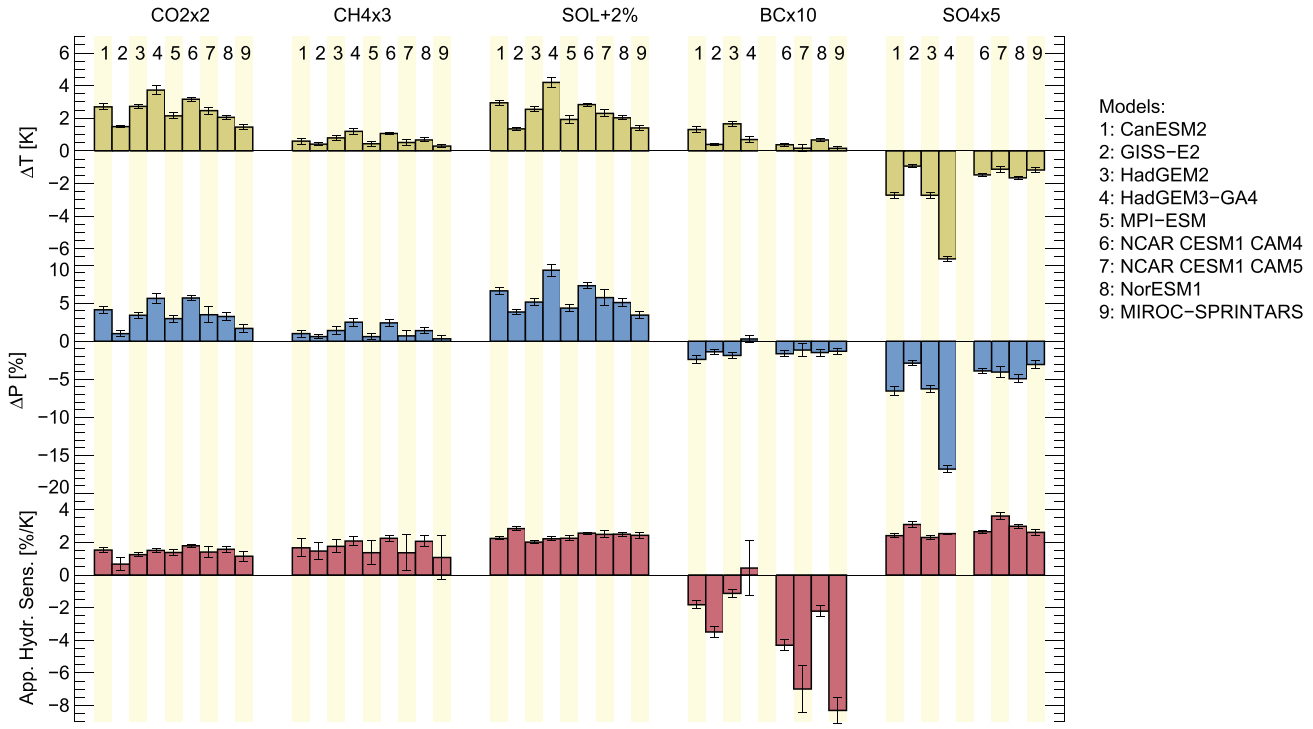

Figure 1. Global, annual mean (top row) temperature and (middle row) precipitation change for years 51–100 following a climate perturbation and (bottom row) the resulting apparent hydrological sensitivity. The numbers indicate the participating models. Error bars indicate ±1 standard deviation of interannual variability.

present models equilibrate well within 5 years of *f*SST running [see, e.g., *Kvalevåg et al*., 2013]. A Gregory-style regression was also performed [*Gregory and Webb*, 2008], regressing the global, annual mean flux change relative to the baseline simulation against the change in surface air temperature (ΔTS) in the coupled simulations. Both methods yield comparable results—see supporting information.

Temperature and precipitation responses to the perturbations were calculated as averages of annual means from the last 10 years of *f*SST simulations or the last 50 years of the coupled simulations. The time windows were chosen to allow both for approximate model equilibration (see section 4) and to encompass internal annual and decadal variability. For the regional analyses, all modeled precipitation responses were regridded to 1° × 1° resolution.

To diagnose the fast precipitation response due to rapid adjustments, ΔP_{fast}, we used the response in the *f*SST simulations. In the coupled simulations, we have assumed that the response over the last 50 years is a linear combination of the fast response and a slow response due to surface temperature change. Hence, the slow response can be calculated as $\Delta P_{\text{slow}} = \Delta P_{\text{total}} - \Delta P_{\text{fast}}$.

3. Results

We first compare the near-surface temperature change and total (fast + slow) precipitation responses to the five climate perturbations, regionally and globally averaged, for all participating models. We then highlight similarities and differences across the multimodel ensemble and for each forcing agent for RF, fast and slow precipitation responses, and contrasts in behavior between land and ocean.

Figure 1 shows the global mean temperature and precipitation responses to the climate perturbations. For *CO2x2*, the temperature response varies between about 2–4 K, consistent with the range in modeled climate sensitivities found in CMIP5 [*Andrews et al*., 2012]. We note, however, that most models have not achieved equilibrium 100 years after the perturbation, and hence, the full temperature response is likely higher. The precipitation response to *CO2x2* ranges from 1 to 6%, correlated with the temperature response. Figure 1 (bottom left) illustrates this, showing the hydrological sensitivity (HS) for *CO2x2* across the models. The HS, defined as $\Delta P_{\text{total}}/\Delta T$ (in recent publications termed the apparent hydrological sensitivity parameter

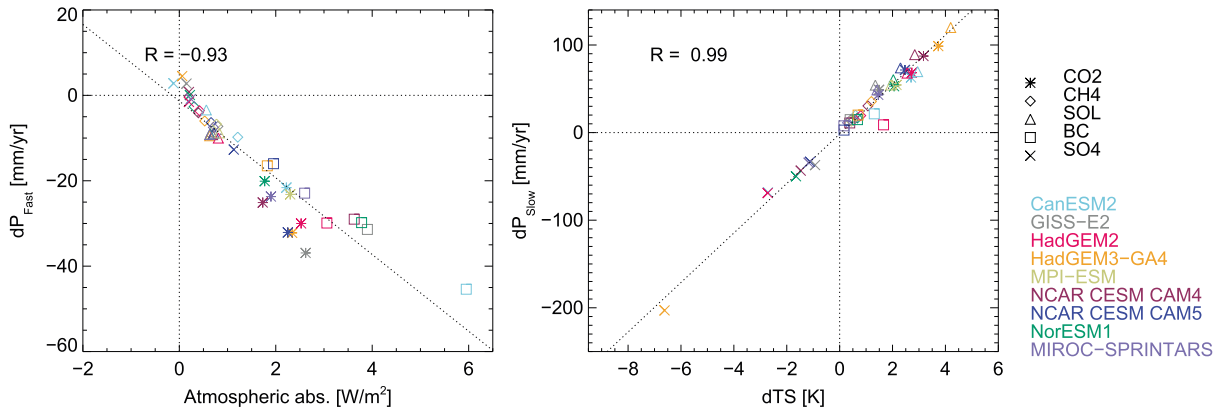

Figure 2. Regression of (left) fast precipitation change versus atmospheric absorption and (right) slow precipitation change versus surface temperature change. The shown regression lines and Pearson coefficients of correlation (*R*) are for the combined data from all models and climate perturbations.

[*Fläschner et al*., 2016], a terminology which we adopt here) shows much less spread, with a multimodel mean HS of 1.4 ± 0.3%/K for *CO2x2*. The error indicates one standard deviation across the present model sample. One model (GISS-E2) stands out as having a markedly lower response than the others, in temperature, precipitation, and HS. This is consistent with this model having among the lowest equilibrium climate sensitivities of the CMIP5 models [*Forster et al*., 2013] and being flagged as an outlier in another recent multimodel study investigating CO_2 forcing in CMIP5 [*DeAngelis et al*., 2015].

For *CH4x3* and *Sol + 2%* the pattern between models is qualitatively similar to *CO2x2*, although the apparent HS is higher: 1.7 ± 0.4%/K for *CH4x3* and 2.4 ± 0.2%/K for *Sol + 2%*. This is in line with earlier modeling studies [*Allen and Ingram*, 2002].

Black carbon shows an opposite precipitation response to the other forcing agents; i.e., it has a negative apparent HS, due to its strong atmospheric absorption of shortwave radiation. All models give a positive temperature response in the *BCx10* case, but with a relatively large spread. The precipitation response is consistently negative, except in one model (HadGEM3-GA4) where it is consistent with zero. The apparent HS for *BCx10* shows sizeable spread.

The sulfate perturbation yields a negative response in both temperature and precipitation, across all models. The HS for *SO4x5* is similar to that for *Sol + 2%* and stronger than for the greenhouse gases. One model (HadGEM3-GA4) finds a markedly strong response to *SO4x5* in both temperature and precipitation but has a HS in line with the other models. This model version simulates a relatively high sulfate aerosol optical depth per unit mass and has previously been shown to have a strong indirect aerosol effect relative to comparable models [*Wilcox et al*., 2015]. NCAR CESM CAM4, which does not include any indirect aerosol effects on clouds, has a sulfate response and a HS that is well within the multimodel spread.

Inspired by earlier single-model studies [*Andrews et al*., 2010; *Kvalevåg et al*., 2013], we investigate correlations of precipitation changes with energetic quantities (Figure 2). Figure 2 (left) shows the regressed change in net atmospheric absorption against the global mean fast precipitation response. RF values were calculated using the *f*SST method. Figure S1 shows the corresponding results when using 20 year Gregory regressions. As in the previous single-model studies, we find a strong negative correlation. The main reason for this is that the greater the change in absorption through the atmospheric column, the more convection is suppressed, leading to reduced precipitation and latent heating. All models show atmospheric absorption consistent with zero for *SO4x5* (except one model, CAM5, which calculates 1 W m^{-2}) and around 0.5 W m^{-2} for *CH4x3* and *Sol + 2%*. *CO2x2* results in around 2 to 3 W m^{-2} of atmospheric absorption for all models, with a corresponding fast precipitation response of −20 to −40 mm/yr. *BCx10* displays significant absorption in all models, but with a very large range, from 1 to more than 5 W m^{-2}. The resulting fast precipitation response, however, largely follows the multimodel, multiperturbation regression line. Deviations from this regression line can occur because the change in the atmospheric energy budget also depends on changes in surface sensible heat flux, as well as the radiative and latent heat terms [see, e.g., *Fläschner et al*., 2016].

Figure 2 (right) regresses the change in near-surface temperature (ΔTS) against the slow precipitation response. We find a strong positive correlation, again in line with previous single-model studies. The results for a single driver show a spread in accordance with the climate sensitivities of the PDRMIP model sample (generally the same versions as in CMIP5 [see *Forster et al*., 2013]). For *BCx10* two models (CanESM2 and HadGEM2) fall well outside the correlation line; however, the temperature change due to the BC perturbation used here is also very low (<2 K for all models). The HadGEM3-GA4 response to *SO4x5* stands out as particularly strong but still follows the general trend.

Broadly, Figure 2 confirms the physical picture drawn in *Andrews et al*. [2010] and *Kvalevåg et al*. [2013]. The precipitation response to a global climate driver can be subdivided into two broad components: A fast response, which scales with changes in the atmospheric absorption, and a slower response related to changes in surface temperature, scaling with the surface temperature change (and, more broadly, TOA RF). Intermodel differences are, however, significant. The scaling with climate sensitivity in Figure 2 (right) is far from perfect, and Figure 2 (left) indicates a wide range of modeled atmospheric absorptions and fast responses for comparable perturbations. Investigating the internal processes that link TOA RF, surface temperature change, and atmospheric absorption to precipitation change in these models therefore is a promising way to understand intermodel spread and potentially reduce multimodel uncertainty in precipitation.

Table S2 lists the multimodel average global mean responses to the five perturbations, for radiative forcing, temperature, and total, fast, and slow precipitation. The PDRMIP ensemble confirms earlier model studies indicating a stronger apparent hydrological sensitivity for changes to solar irradiance (2.4%/K) relative to the greenhouse gases (1.4%/K). Further, the modeled climates are also more sensitive to aerosol perturbations than to forcing from greenhouse gases, albeit with a significantly higher ensemble uncertainty for *BCx10*. Recent publications have studied how the precipitation response to a climate driver scales with surface temperature change alone, termed the slow hydrological sensitivity [e.g., *Andrews et al*., 2010; *Fläschner et al*., 2016], and found that it varies less between models and drivers than the apparent HS. This will be explored for the PDRMIP model ensemble in an upcoming publication.

Figure 3 shows the multimodel mean geographical patterns of the total, fast, and slow precipitation responses to the individual perturbations. For most regions and perturbations, the models do not all agree on the sign of the responses; however, some robust features are still apparent.

For *CO2x2* (Figure 3, top row), the total response is composed of a negative fast response at most latitudes and a stronger positive slow response at all latitudes but with a few exceptions in the Intertropical Convergence Zone (ITCZ) regions. The former is mainly due to the stabilizing effect of the atmospheric absorption of CO_2 and the latter due to the gradual increase in surface temperature. The total precipitation change is strongest around the equator, dominated by the slow change over the Pacific Ocean. Most regions are dominated by the slow response, but some land regions are dominated by the fast changes (see below).

CH4x3 and *Sol + 2%* (Figure 3, second and third rows) show broadly similar total and slow precipitation response features to *CO2x2*, except that *CH4x3* has lower absolute response due to the weaker RF (as also seen in Figure 1). The model mean fast response to *CH4x3* is nonsignificant for all latitudes, as expected for climate perturbations with low atmospheric absorption. *SO4x5* (Figure 3, bottom row) shows an inverted pattern to the solar and greenhouse gas perturbations, with virtually no (significant) fast response in the zonal mean. For *CO2x2*, *CH4x3*, *Sol + 2%*, and *SO4x5*, there is a clear land/ocean difference, in line with earlier analyses based on the CMIP5 model ensemble [*Richardson et al*., 2016]. Tropical land areas generally see a positive fast precipitation response, largely canceled out in the zonal and global means by a corresponding negative response over tropical oceans.

BCx10 (Figure 3, fourth row) shows a markedly different response pattern to the other perturbations. There is little slow response, except in the tropics where the zonal mean shows a small positive precipitation change north of the equator and a smaller negative one south of the equator. The total is dominated by the fast response, which is generally negative at most latitudes. The aerosol perturbations tend to shift the ITCZ more (southward for *SO4x5* and north for *BCx10*) than the solar and greenhouse gas changes, due to the more hemispherically heterogeneous RF that they cause.

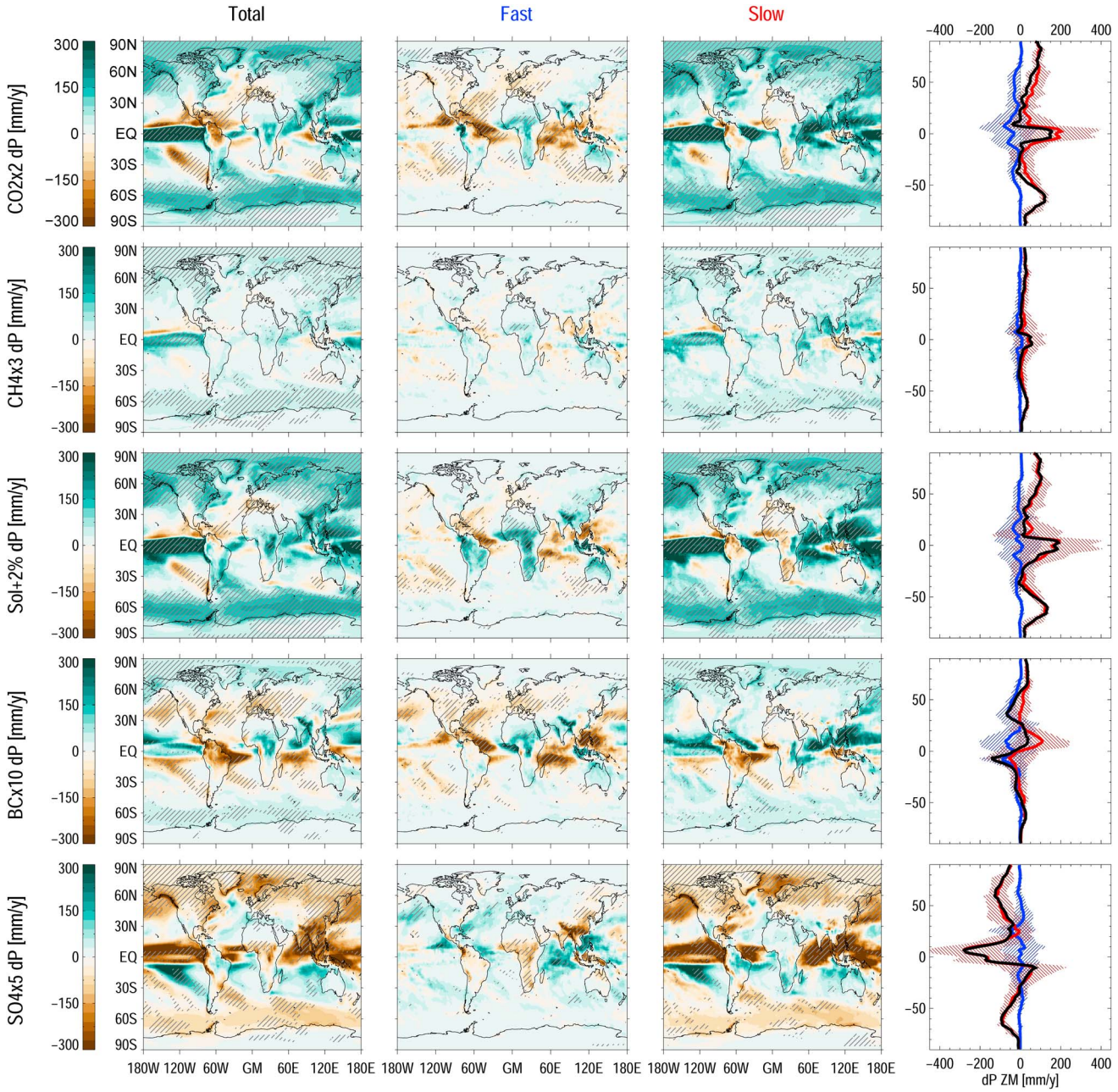

Figure 3. Geographical patterns of multimodel mean precipitation change. Each row shows a different climate perturbation. Hatched regions indicate where the multimodel mean is more than 1 standard deviation away from zero. (first column) Total change. (second column) Fast change due to rapid adjustments. (third column) Slow change due to surface temperature change. (fourth column) Multimodel zonal means, showing fast (blue), slow (red), and total (black) precipitation changes. The shaded bands show $\pm 1\sigma$ of the nine-model ensemble.

A common misconception about the change in precipitation caused by a given driver is that it is composed of an initial, weak fast response due to rapid adjustments, which will over time be overwhelmed by the slow, temperature-driven response. Figure 3, however, indicates that in several regions, the fast response may dominate even when the climate system approaches a new equilibrium, in line with what has previously been observed for tropical precipitation under rising CO_2 concentrations [*Bony et al.*, 2013]. In Figure 4 (top row) we explore this by comparing the total, fast, and slow precipitation responses over land and ocean separately and over six land regions: North America, South America, Europe, Africa, South Asia, and Australia (for region definitions, see Figure S2). There are clearly large regional and intermodel differences, but some significant features still emerge. Over the ocean, the climate drivers cause a fast response opposed by a slow

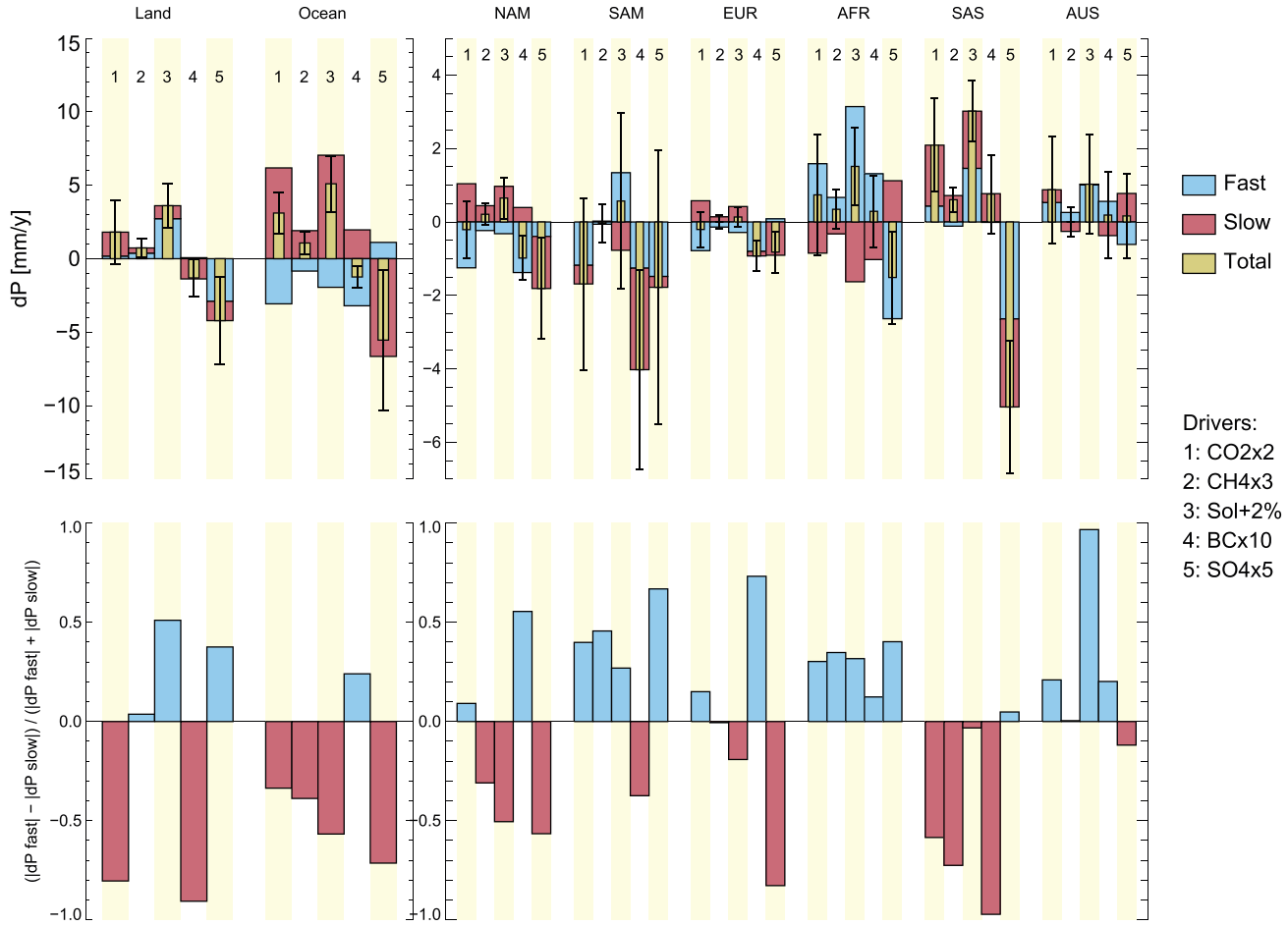

Figure 4. (top row) Regional precipitation response, divided into fast and slow components for five climate drivers. (left column) Land and ocean responses. (right column) Response for the land-only regions of North America (NAM), South America (SAM), Europe (EUR), Africa (AFR), the major aerosol emission regions of South Asia (SAS), and Australia (AUS). See Figure S2 for definitions. (bottom row) Response ratio (see text), calculated from the multimodel mean values in Figure 4 (the top row).

response. Over some land regions, however, the fast and slow responses have the same sign. This signature is particularly clear over South Asia.

To determine whether fast or slow precipitation responses dominate over years 51–100 of the PDRMIP simulations, we define the response ratio $R_{resp} = (|\Delta P_{fast}| - |\Delta P_{slow}|)/(|\Delta P_{fast}| + |\Delta P_{slow}|)$. R_{resp} will be positive when rapid adjustments dominate the long-term precipitation response and negative when the slow response dominates. For the extreme cases of only fast or slow responses, R_{resp} will be +1 or −1, respectively. Figure 4 (bottom row) shows the multimodel mean R_{resp} for all PDRMIP drivers, for land, ocean, and the six regions defined above. For most regions and drivers, the models do not consistently agree on the dominating response (not shown). The response over oceans is, however, consistently dominated by the slow response for all drivers and models, except for *BCx10* where all models but one predict that the fast precipitation response still dominates at near equilibrium. Considering land regions, South America and Africa are mainly dominated by the fast response for all perturbations. Australia shows a similar pattern, albeit with a much larger intermodel spread. Southeast Asia sees a dominance of the slow response, while North America and Europe have a more mixed response to the different drivers. The latter mainly reflects a large intermodel spread in the results, probably at least partly due to differences in aerosol treatment and lifetime (where emissions were used) for the *BCx10* and *SO4x5* cases. For the *CO2x2* case, one factor likely contributing to the dominance of fast responses over land is the physiological forcing from CO_2-induced stomatal response, which has been shown to significantly affect both surface temperature response and water balance in previous model studies [*Cao et al.*, 2010].

4. Discussion

Overall, the results presented in the previous section agree with earlier single-model studies of the precipitation impacts of individual forcers and confirm our expectations based on simple energetics. The internal mechanisms linking changes to the energy balance to altered precipitation rates, however, differ between models, and we do see significant intermodel variability.

The hydrological sensitivity for a *BCx10* perturbation varies strongly between models. One model even shows a positive (nonsignificant) apparent HS. This is likely due to the multiple ways in which BC can affect climate—directly, through absorption and scattering of incoming sunlight; indirectly, through modifications of cloud microphysical properties; and semidirectly, through heating ambient air and thus altering stability and/or burning off clouds from within [*Bond et al*., 2013; *Samset and Myhre*, 2015]. This range of effects is much larger than, e.g., for *SO4x5*, where the additional particles mainly scatter incoming sunlight and affect cloud microphysics. BC-climate interactions are treated very differently in present global climate models, as are transport and removal processes, factors which cause strong variations even for direct radiative forcing [see, e.g., *Samset et al*., 2013]. For example, it is interesting to note that the responses for HadGEM2 and HadGEM3-GA4 are markedly different, even though they use the same aerosol physics schemes. Also, some models have used prescribed concentrations based on AeroCom Phase II, and some have used native emissions. As we have not attempted to normalize the responses to the simulated aerosol burden, or to any differences in vertical profile, this is one likely contributor to the observed diversity [*Ban-Weiss et al*., 2011; *Hodnebrog et al*., 2014; *Samset and Myhre*, 2015]. The precipitation response to BC perturbations in PDRMIP will be investigated in detail in a follow-up publication. We note that the differences seen here will have been present for CMIP5, meaning that BC is likely a strong contributor to the prediction diversity seen there.

As noted above, most PDRMIP models ran their coupled simulations with a fully coupled ocean. This means that for strong perturbations like *CO2x2*, they will likely not have reached their equilibrium warming within the 100 years simulated here. Recently, *Caldeira and Myhrvold* [2013] found that in the CMIP5 model ensemble, on average 80% of the equilibrium warming after a $4xCO_2$ perturbation had been realized after the first 100 simulation years. One PDRMIP model (GISS-E2) ran an additional 250 years for our *CO2x2* case and found an additional 0.5 K warming beyond the 1.5 K realized over their first 100 years. Another (CanESM2) found an additional 0.6 K beyond the 2.7 K in the first 100 years when running the model for 800 years. Both of these results are consistent with the *Caldeira and Myhrvold* [2013] analysis, indicating that we could expect similar extra, long-term warming for the other models in the PDRMIP ensemble. For the present analysis, this nonequilibrium is not crucial for the main conclusions, as models are then well within the regimes where changes to precipitation scale with the slow increase in surface temperature. Hence, for fully equilibrated models both the temperature and precipitation responses to the perturbations would have been stronger but still follow the trends shown in Figure 2. The ratio of fast to slow precipitation response would, however, likely change on such long time scales, changing the regional patterns found in Figures 3 and 4.

A further potential issue with the present analysis is the temperature response over land in the *f*SST simulations. In principle, the fast response as diagnosed above could have a slow component, as the land surface temperature may increase somewhat with time even if sea surface temperatures are kept constant. We tested the impact of this by calculating the global mean temperature change over land in the *f*SST case, assuming a resulting precipitation change of $(\Delta P_{\mathrm{slow}}/\Delta T_{\mathrm{land,coupled}}) \times \Delta T_{\mathrm{land},f\mathrm{SST}}$ and reinterpreting it as part of the slow response. While this procedure changes the results by up to 10% for some models, the multimodel mean results presented above are not affected within the uncertainties given.

5. Conclusions

We have presented the response to perturbations to five climate forcers (*CO2x2*, *CH4x3*, *Sol + 2%*, *BCx10*, and *SO4x5*) across nine global climate models, as part of the PDRMIP project. As in previous single-model studies, we find that global mean precipitation responds on two time scales: one fast response, acting on the time scale of months, that scales closely with the atmospheric energy net absorption due to the forcing agent and a slower response that scales with the long-term change in global surface temperature. All models show

broadly similar responses to the perturbations, but beyond this there is still significant intermodel variability, indicating differences in how the atmosphere reacts to altered absorption and surface temperature. Black carbon stands out as the forcing agent with the largest intermodel spread in hydrological sensitivity. The precipitation response over oceans is quite uniform between models and dominates the global mean values. Over land, where the precipitation response to climate drivers is arguably much more relevant for human activities, we find large regions where the rapid adjustments dominate over the slow response across the entire model ensemble, even 100 years after the perturbation was applied. The main results in the present paper will be further explored in upcoming PDRMIP publications, with emphasis on hydrological sensitivities, energy balances, circulation changes, and radiative forcing.

Acknowledgments

All model results used for the present study are available to the public through the Norwegian NORSTORE data storage facility. B.H.S., G.M., and Ø.H. were funded by the Research Council of Norway, through the grant NAPEX (229778). Supercomputer facilities were generously provided by NOTUR. D.S. thanks the NASA High-End Computing Program through the NASA Center for Climate Simulation at Goddard Space Flight Center for computational resources. M.K. and A.V. are supported by the Natural Environment Research Council under grant NE/K500872/1. Simulations with HadGEM3-GA4 were performed using the MONSooN system, a collaborative facility supplied under the Joint Weather and Climate Research Programme, which is a strategic partnership between the Met Office and the Natural Environment Research Council. T.T. was supported by the supercomputer system of the National Institute for Environmental Studies, Japan, the Environment Research and Technology Development Fund (S-12-3) of the Ministry of the Environment, Japan, and JSPS KAKENHI grants 15H01728 and 15 K12190. D.J.L.O. and A.K. were supported by the Norwegian Research Council through the projects EVA (grant 229771) and EarthClim (207711/E10), NOTUR (nn2345k), and NorStore (ns2345k) projects. T.R. was supported by NERC training award NE/K007483/1 and acknowledges the use of the MONSooN system. Computing resources for J.F.L. (ark:/85065/d7wd3xhc) were provided by the Climate Simulation Laboratory at NCAR's Computational and Information Systems Laboratory, sponsored by the National Science Foundation and other agencies. Computing resources for the simulations with the MPI model were provided by the German Climate Computing Center (DKRZ), Hamburg. TA was supported by the Joint UK DECC/Defra Met Office Hadley Centre Climate Programme (GA01101).

References

Allen, M. R., and W. J. Ingram (2002Constraints on future changes in climate and the hydrologic cycle), *Nature*, *419*(6903), 224–232.

Andrews, T., and P. M. Forster (2010), The transient response of global-mean precipitation to increasing carbon dioxide levels, *Environ. Res. Lett.*, *5*(2), 025212, doi:10.1088/1748-9326/5/2/025212.

Andrews, T., P. M. Forster, O. Boucher, N. Bellouin, and A. Jones (2010), Precipitation, radiative forcing and global temperature change, *Geophys. Res. Lett.*, *37*, L14701, doi:10.1029/2010GL043991.

Andrews, T., J. M. Gregory, M. J. Webb, and K. E. Taylor (2012), Forcing, feedbacks and climate sensitivity in CMIP5 coupled atmosphere-ocean climate models, *Geophys. Res. Lett.*, *39*, L09712, doi:10.1029/2012GL051607.

Bala, G., K. Caldeira, and R. Nemani (2010), Fast versus slow response in climate change: Implications for the global hydrological cycle, *Clim. Dyn.*, *35*(2–3), 423–434, doi:10.1007/s00382-009-0583-y.

Ban-Weiss, G. A., L. Cao, G. Bala, and K. Caldeira (2011), Dependence of climate forcing and response on the altitude of black carbon aerosols, *Clim. Dyn.*, *38*(5–6), 897–911, doi:10.1007/s00382-011-1052-y.

Bond, T. C., et al. (2013), Bounding the role of black carbon in the climate system: A scientific assessment, *J. Geophys. Res. Atmos.*, *118*, 5380–5552, doi:10.1002/jgrd.50171.

Bony, S., G. Bellon, D. Klocke, S. Sherwood, S. Fermepin, and S. Denvil (2013), Robust direct effect of carbon dioxide on tropical circulation and regional precipitation, *Nat. Geosci.*, *6*(6), 447–451, doi:10.1038/ngeo1799. [Available at http://www.nature.com/ngeo/journal/v6/n6/abs/ngeo1799.html#supplementary-information.]

Boucher, O., et al. (2013), Clouds and aerosols, in *Climate Change 2013: The Physical Science Basis. Contribution of Working Group I to the Fifth Assessment Report of the Intergovernmental Panel on Climate Change*, edited by T. F. Stocker et al., pp. 571–658, Cambridge Univ. Press, Cambridge, U. K., and New York.

Caldeira, K., and N. P. Myhrvold (2013), Projections of the pace of warming following an abrupt increase in atmospheric carbon dioxide concentration, *Environ. Res. Lett.*, *8*(3), 034039.

Cao, L., G. Bala, K. Caldeira, R. Nemani, and G. Ban-Weiss (2010), Importance of carbon dioxide physiological forcing to future climate change, *Proc. Natl. Acad. Sci. U.S.A.*, *107*(21), 9513–9518, doi:10.1073/pnas.0913000107.

Cao, L., G. Bala, and K. Caldeira (2012), Climate response to changes in atmospheric carbon dioxide and solar irradiance on the time scale of days to weeks, *Environ. Res. Lett.*, *7*(3), 034015.

Collins, M., et al. (2013), Long-term climate change: Projections, commitments and irreversibility, in *Climate Change 2013: The Physical Science Basis. Contribution of Working Group I to the Fifth Assessment Report of the Intergovernmental Panel on Climate Change*, edited by T. F. Stocker et al., pp. 1029–1136, Cambridge Univ. Press, Cambridge, U. K., and New York.

DeAngelis, A. M., X. Qu, M. D. Zelinka, and A. Hall (2015), An observational radiative constraint on hydrologic cycle intensification, *Nature*, *528*(7581), 249–253, doi:10.1038/nature15770.

Fläschner, D., T. Mauritsen, and B. Stevens (2016), Understanding the intermodel spread in global-mean hydrological sensitivity, *J. Clim.*, *29*(2), 801–817, doi:10.1175/jcli-d-15-0351.1.

Forster, P. M., T. Andrews, P. Good, J. M. Gregory, L. S. Jackson, and M. Zelinka (2013), Evaluating adjusted forcing and model spread for historical and future scenarios in the CMIP5 generation of climate models, *J. Geophys. Res. Atmos.*, *118*, 1139–1150, doi:10.1002/jgrd.50174.

Gregory, J., and M. Webb (2008), Tropospheric adjustment induces a cloud component in CO_2 forcing, *J. Clim.*, *21*(1), 58–71, doi:10.1175/2007JCLI1834.1.

Hartmann, D. L., et al. (2013), Observations: Atmosphere and surface, in *Climate Change 2013: The Physical Science Basis. Contribution of Working Group I to the Fifth Assessment Report of the Intergovernmental Panel on Climate Change*, edited by T. F. Stocker et al., pp. 159–254, Cambridge Univ. Press, Cambridge, U. K., and New York.

Hodnebrog, Ø., G. Myhre, and B. H. Samset (2014), How shorter black carbon lifetime alters its climate effect, *Nat. Commun.*, *5*, 5065, doi:10.1038/ncomms6065.

Kamae, Y., and M. Watanabe (2012), Tropospheric adjustment to increasing CO_2: Its timescale and the role of land–sea contrast, *Clim. Dyn.*, *41*(11–12), 3007–3024, doi:10.1007/s00382-012-1555-1.

Knutti, R., and J. Sedláček (2012), Robustness and uncertainties in the new CMIP5 climate model projections, *Nat. Clim. Change*, *3*(4), 369–373, doi:10.1038/nclimate1716.

Kvalevåg, M. M., B. H. Samset, and G. Myhre (2013), Hydrological sensitivity to greenhouse gases and aerosols in a global climate model, *Geophys. Res. Lett.*, *40*, 1432–1438, doi:10.1002/grl.50318.

Myhre, G., et al. (2013a), Anthropogenic and natural radiative forcing, in *Climate Change 2013: The Physical Science Basis. Contribution of Working Group I to the Fifth Assessment Report of the Intergovernmental Panel on Climate Change*, edited by T. F. Stocker et al., pp. 659–740, Cambridge Univ. Press, Cambridge, U. K., and New York.

Myhre, G., et al. (2013b), Radiative forcing of the direct aerosol effect from AeroCom Phase II simulations, *Atmos. Chem. Phys.*, *13*(4), 1853–1877, doi:10.5194/acp-13-1853-2013.

O'Gorman, P., R. Allan, M. Byrne, and M. Previdi (2012), Energetic constraints on precipitation under climate change, *Surv. Geophys.*, *33*(3–4), 585–608, doi:10.1007/s10712-011-9159-6.

Richardson, T. B., P. M. Forster, T. Andrews, and D. J. Parker (2016), Understanding the rapid precipitation response to CO_2 and aerosol forcing on a regional scale, *J. Clim.*, *29*(2), 583–594, doi:10.1175/jcli-d-15-0174.1.

Samset, B. H., and G. Myhre (2015), Climate response to externally mixed black carbon as a function of altitude, *J. Geophys. Res. Atmos.*, *120*, 2913–2927, doi:10.1002/2014JD022849.

Samset, B. H., et al. (2013), Black carbon vertical profiles strongly affect its radiative forcing uncertainty, *Atmos. Chem. Phys.*, *13*(5), 2423–2434, doi:10.5194/acp-13-2423-2013.

Sherwood, S. C., S. Bony, O. Boucher, C. Bretherton, P. M. Forster, J. M. Gregory, and B. Stevens (2015), Adjustments in the forcing-feedback framework for understanding climate change, *Bull. Am. Meteorol. Soc.*, *96*(2), 217–228, doi:10.1175/bams-d-13-00167.1.

Wilcox, L. J., E. J. Highwood, B. B. B. Booth, and K. S. Carslaw (2015), Quantifying sources of inter-model diversity in the cloud albedo effect, *Geophys. Res. Lett.*, *42*, 1568–1575, doi:10.1002/2015GL063301.